Stable Atomic Magnetometer in Parity-Time Symmetry Broken Phase

Xiangdong Zhang, Jinbo Hu, and Nan Zhao*
Beijing Computational Science Research Center

(Received 4 April 2022; accepted 15 November 2022; published 9 January 2023)

Random motion of spins is usually detrimental in magnetic resonance experiments. The spin diffusion in nonuniform magnetic fields causes broadening of the resonance and limits the sensitivity and the spectral resolution in applications like magnetic resonance spectroscopy. Here, by observation of the parity-time (PT) phase transition of diffusive spins in gradient magnetic fields, we show that the spatial degrees of freedom of atoms could become a resource, rather than harmful, for high-precision measurement of weak signals. In the normal phase with zero or low gradient fields, the diffusion results in dissipation of spin precession. However, by increasing the field gradient, the spin system undergoes a PT transition, and enters the PT symmetry broken phase. In this novel phase, the spin precession frequency splits due to spatial localization of the eigenmodes. We demonstrate that, using these spatial-motion-induced split frequencies, the spin system can serve as a stable magnetometer, whose output is insensitive to the inevitable long-term drift of control parameters. This opens a door to detect extremely weak signals in imperfectly controlled environments.

DOI: 10.1103/PhysRevLett.130.023201

Introduction.—Measurement of extremely weak signals requires sensors with high sensitivity and high stability. High sensitivity allows the sensor to generate a large enough signal against background noise. However, the signal-to-noise ratio is ultimately limited by the measurement time. During a long measurement, even if the detected signal is actually unchanged, the sensor output is prone to vary over time due to the imperfect control of measurement conditions (e.g., the low frequency drift of electronic devices). In this sense, the ability of rejection or compensation of long-term drift, i.e., the stability, of a sensor is essential for measuring extremely weak signals.

Atomic spins are useful in the sensing of weak magnetic fields [1] or signals which are regarded as effective magnetic fields, such as inertial rotations [2] and extraordinary interactions of fundamental physics [3–7]. These fields to be detected will manifest themselves by shifting the precession frequency of atomic spins. For atoms in liquid or gas phases, their spatial motion is usually governed by the diffusion law. With inevitable magnetic field inhomogeneity, the diffusion causes spin relaxation and decoherence, which increase the uncertainty of the spin precession frequency and degrade the weak field sensing.

The spin precession with spatial motion was extensively studied decades ago [8–10]. The dynamics of diffusive atomic spins is governed by the Torrey equation [10]. When confined in a finite volume, the atomic motion is described by a series of eigenmodes with complex eigenvalues. Stoller, Happer and Dyson [11] gave the exact solution to the Torrey equation with a linear magnetic field gradient and demonstrated the branch behavior of the eigenvalue spectrum due to the non-Hermitian nature of the Torrey equation.

The spin diffusion in nonuniform magnetic field is an ideal platform for studying the non-Hermitian physics. The branch spectrum of the Torrey equation proposed in Ref. [11] is indeed the signature of the PT transition [12,13]. Among a number of experimental demonstrations of the PT transition in various physical systems [14–23], Zhao, Schaden and Wu [24–28] observed the PT transition

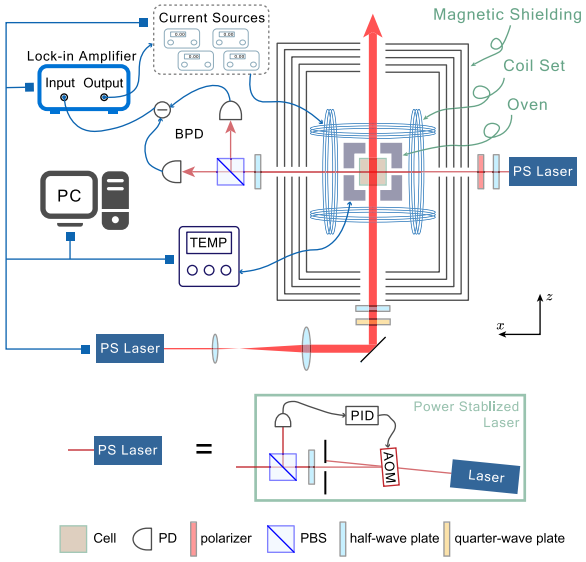

FIG. 1. Experimental setup. A cubic glass cell containing Xe gas and Rb metal is placed inside a magnetic shielding and heated. A parametric magnetometer [37–41] is used to detect the nuclear spin signals. See Sec. I of the Supplemental Material [42] for more details.

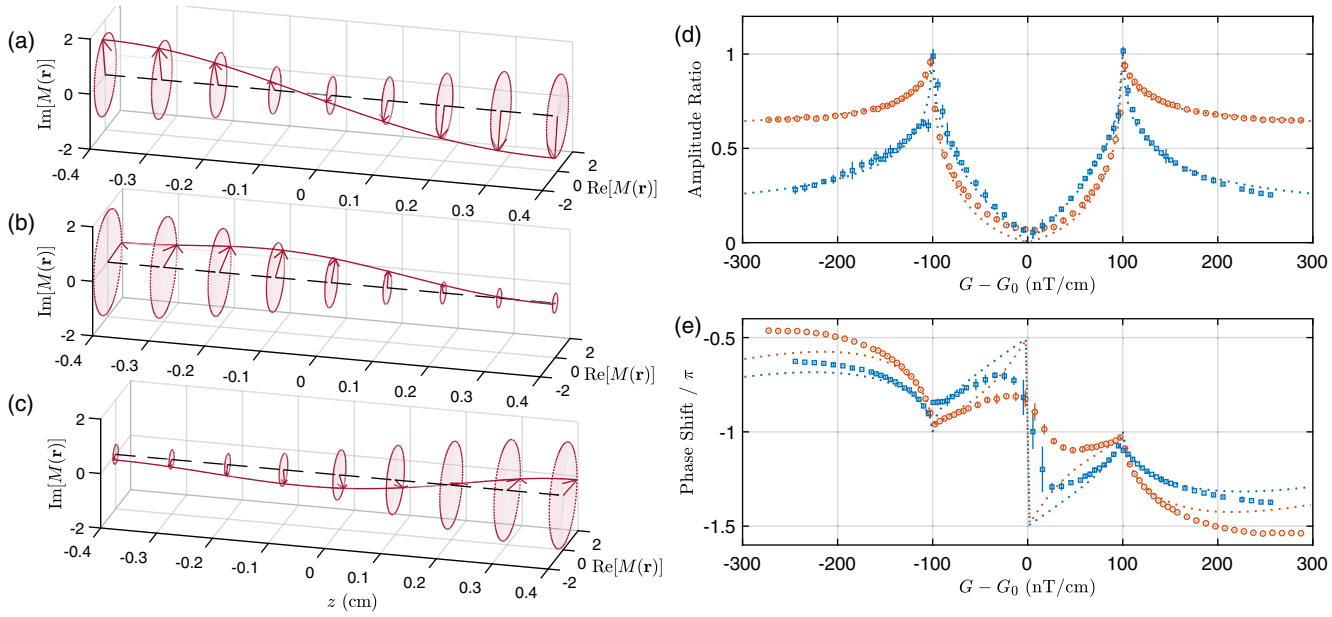

FIG. 2. Spatial distribution of the eigenmodes of the Torrey equation. (a) The distribution of $M_+(z)$ in PT-symmetric phase with $G = 80$ nT/cm. The eigenmode $M_-(z)$ is nearly uniform along the z direction. (b),(c) Similar to (a) but for $M_\pm(z)$ in PT-broken phase with $G = 250$ nT/cm. (d),(e) The amplitude ratio $\eta(G; z_p)$ and the phase shift $\delta\theta(G; z_p)$ at different probe beam positions. $\delta\theta \equiv \theta_+ - \theta_-$ for the PT-symmetric phase and the PT-broken phase with $G < 0$; $\delta\theta \equiv \theta_- - \theta_+$ for the PT-broken phase with $G > 0$. The symbols are measured data points extracted from the FID spectrum. The displacement of the probe beam in our experiment is $z_{p,red} - z_{p,blue} = 1.18 \pm 0.02$ mm. The dashed lines are theoretical results using the same parameters as in Fig. 3 and with probe beam positions $z_{p,red} = -0.56$ mm and $z_{p,blue} = -1.74$ mm. The red (blue) data points are the mean value of five (three) repeated measurements. The error bars [50] in the PT-symmetric phase may be underestimated; see Sec. III D of the Supplemental Material [42].

in a system of diffusive electron spin of Rb atoms using ultrathin vapor cells. Here, we study the PT transition process of diffusive nuclear spins. The full eigenvalue spectrum in both PT-symmetric and PT-broken phases and, particularly, the mode localization (also known as edge-enhancement [29]) behavior in the PT-broken phase are observed.

We further demonstrate the application of the PT transition of diffusive spins in magnetometry. In contrast to previous studies on the improvement of sensitivity near the exceptional points (EPs) [30–36], we show that the spatial motion of spins in the PT-broken phase could be a resource for improving measurement stability.

PT transition of diffusive spins.—We observe the PT transition of diffusive nuclear spins by using the experimental setup shown in Fig. 1. Two isotopes of noble gas (^{129}Xe and ^{131}Xe), both carrying nuclear spins, are sealed in a cubic glass cell with inner side length $L = 0.8$ cm. The free-induction decay (FID) signal of the Xe nuclear spins is measured to explore their dynamics.

The dynamics of the Xe nuclear spins is governed by the Torrey equation [10]

$$\frac{\partial K_+(\mathbf{r},t)}{\partial t} = D\nabla^2 K_+(\mathbf{r},t) - (i\gamma B_z + \Gamma_{2c})K_+(\mathbf{r},t), \quad (1)$$

where $K_+(\mathbf{r},t) \equiv K_x + iK_y$ is the transverse component of the Xe nuclear spin magnetization $\mathbf{K}(\mathbf{r},t)$, D is the diffusion constant, γ is the gyromagnetic ratio of Xe nuclear spins, $B_z(\mathbf{r})$ is the magnetic field along the z direction, and Γ_{2c} is the intrinsic spin relaxation rate due to interatom collisions. We present a detailed solution of Eq. (1) in Sec. II of the Supplemental Material [42].

Consider the special case where $B_z(\mathbf{r}) = B_0 + G \cdot z$ and the boundary condition is $\hat{\mathbf{n}} \cdot \nabla K_+(\mathbf{r}) = 0$ on the cell walls. The eigenproblem corresponding to Eq. (1) can simplify to

$$\left(D\frac{d^2}{dz^2} - i\gamma G \cdot z\right)M_k(z) = -s_k M_k(z), \qquad k = 0, 1, 2, \ldots \quad (2)$$

Here, we ignore the x, y directions because B_z is uniform along these directions, and thus $M_k(\mathbf{r}) = M_k(z)$ for the ground modes. The $i\gamma B_0$ and Γ_{2c} terms are dropped because they only contribute a constant shift to all eigenvalues $\{s_k\}$.

The PT operation changes Eq. (2) into

$$\left(D\frac{d^2}{dz^2} - i\gamma G \cdot z\right)M_k^*(-z) = -s_k^* M_k^*(-z), \quad (3)$$

meaning that both $\{s_k, M_k(z)\}$ and $\{s_k^*, M_k^*(-z)\}$ solve Eq. (2).

In the small gradient region, all $\{s_k\}$ are purely real and no degeneracy exists, which means the eigenmodes should

have PT symmetry, i.e., $M_k(z) = M_k^*(-z)$. Figure 2(a) shows an example of $M_1(z)$ in this region. The eigenmodes extend over the whole cell; mode localization at the boundary is prevented by the PT symmetry.

However, predicted by the solution in Ref. [11], there is a critical gradient called EP where s_0 and s_1 become the same. In the region $|G| > G_{\mathrm{EP}}$, the imaginary part of s_0 and s_1 are nonzero, and the PT symmetry of $M_0(z)$ and $M_1(z)$ breaks. Instead, PT operation transforms $M_0(z)$ into $M_1^*(-z)$. As the gradient gets larger, $M_0(z)$ and $M_1(z)$ start to localize on the opposite ends of the cell. This leads to the splitting of the resonance frequency of these eigenmodes since they "feel" a different average field. Figures 2(b) and 2(c) show an example of $M_0(z)$ and $M_1(z)$ in this region. (For more details, see Sec. II E of the Supplemental Material [42].)

Based on the symmetry of eigenmodes, the $|G| < G_{\mathrm{EP}}$ region is named as the PT-symmetric phase, and the $|G| > G_{\mathrm{EP}}$ region is the PT-broken phase. The theoretical prediction of EP for ^{129}Xe in our experiment is $G_{\mathrm{EP}} = 99.4$ nT/cm. The EP for ^{131}Xe (~335 nT/cm) is larger than the gradient region we can reach.

The evolution of K_+ can be expanded using the eigenmodes as $K_+(\mathbf{r}, t) = \sum_k c_k M_k(\mathbf{r}) e^{-s_k t}$, where $\{c_k\}$ are expansion coefficients determined by the initial spin distribution. The FID signal is proportional to [see Eq. (S40) of the Supplemental Material [42]]

$$K_x(z_{\mathrm{p}}, t) = \sum_{k=0}^{\infty} A_k(z_{\mathrm{p}}) \cos[\omega_k t + \theta_k(z_{\mathrm{p}})] e^{-\Gamma_k t}, \quad (4)$$

where z_{p} is the position of probe beam (on the z axis), $A_k(z_{\mathrm{p}}) \equiv |c_k M_k(z_{\mathrm{p}})|$, $\theta_k(z_{\mathrm{p}}) \equiv -\arg[c_k M_k(z_{\mathrm{p}})]$, and $s_k \equiv \Gamma_k + i\omega_k$. Since higher excited modes decay very fast, only M_0 and M_1 have an experimentally observable effect. In the following, the subscript $k = 1$ and 0 is replaced by "+" and "−" signs, respectively.

Figure 3(a) shows the spectrum of FID signals at various gradient. The resonance peak splits as the gradient gets larger. Figures 3(b) and 3(c) compare the measured eigenvalues $s_\pm$ with the theoretical values. The behavior of $\Gamma_\pm$ and $\omega_\pm$ fits well with theory. Figures 2(d) and 2(e) show the amplitude ratio $\eta(z_{\mathrm{p}}) \equiv A_{\mathrm{min}}/A_{\mathrm{max}}$ and phase shift $\delta\theta(z_{\mathrm{p}}) \equiv \pm(\theta_+ - \theta_-)$ of the two eigenmodes $M_\pm$, where A_{max} (A_{min}) is the larger (smaller) amplitude between $A_\pm(z_{\mathrm{p}})$. Two probe beam positions are used to verify the spatial distribution of eigenmodes. The amplitude ratio η fits well with theory, and is sensitive to z_{p} in the PT-broken phase due to the localization of eigenmodes. The phase shift fits not so good with theory because of the fitting accuracy and the difficulty of determining the precise time origin of a FID signal.

Stable comagnetometer in PT-broken phase.—One can utilize the split spin precession frequencies in the PT-broken phase to stabilize the output of the atomic magnetometers. In general, the precession frequency ω_α of a given

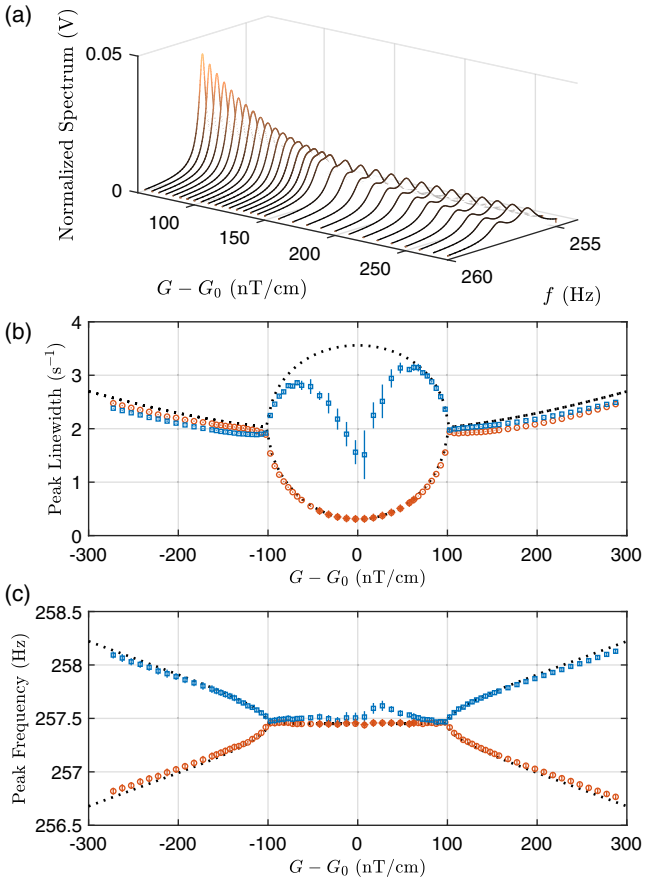

FIG. 3. Eigenvalue spectrum of diffusive spins. (a) Fourier spectrum of measured FID signals of ^{129}Xe as a function of G at pump power 250 mW. (b),(c) The peak linewidth $\Gamma_\pm$ and precession frequency $\omega_\pm/(2\pi)$ of ^{129}Xe spins. The symbols are measured data extracted from the FID spectrum, and the dashed curves are the calculated eigenvalues of Eq. (1) with $|\gamma B_0|/(2\pi) = 257.45$ Hz, $\Gamma_{2c} = 0.306$ s^{-1}, and $D = 0.211$ cm^2/s. The blue data points in the $|G| < 70$ nT/cm region are less reliable due to the fast decay of the excited mode $M_+(z)$ (see Sec. III D of the Supplemental Material [42]). All data points are the mean value of five repeated measurements. See Sec. III of the Supplemental Material [42] for details of FID spectrum fitting.

spin species α is usually influenced by a number of input variables and is expressed by a multivariate function $\omega_\alpha = \omega_\alpha(\mathbf{x})$ of the input vector $\mathbf{x} = [x_1, x_2, \ldots, x_M]^{\mathrm{T}}$. Among the M components of $\mathbf{x}$, only one is the real signal we want to detect (e.g., the unknown magnetic field). The remaining $M - 1$ variables will cause systematic error if they are not well controlled. Comagnetometers use M precession frequencies $\boldsymbol{\omega} = [\omega_1, \omega_2, \ldots, \omega_M]^{\mathrm{T}}$ of different spin species to determine the M variables in $\mathbf{x}$ unambiguously. As long as the Jacobian matrix $J = [\partial\omega_i/\partial x_j]_{i,j=1,\ldots,M}$ of the multidimensional function $\boldsymbol{\omega} = \boldsymbol{\omega}(\mathbf{x})$ is invertible, the comagnetometer is immune to the drift of all the variables in $\mathbf{x}$.

The dual-species nuclear magnetic resonance gyroscope (NMRG) [2], a kind of comagnetometer, uses the

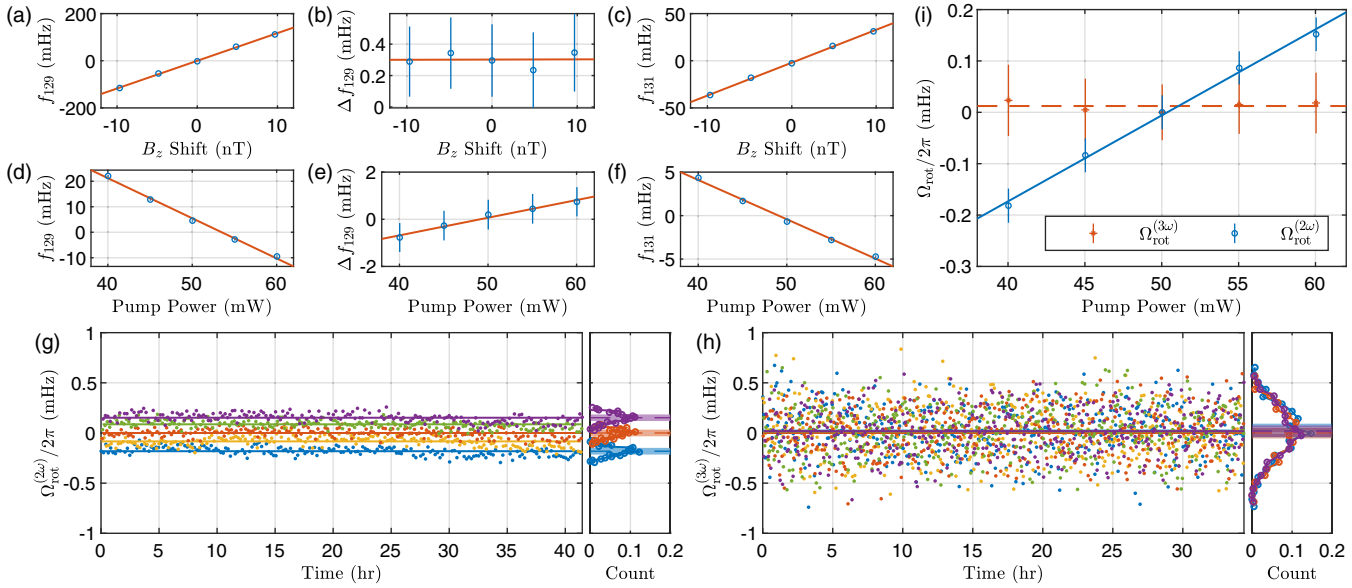

FIG. 4. Stable comagnetometer. (a)–(c) Magnetic field dependence of three measured frequencies. $[f_{129}, \Delta f_{129}, f_{131}] \equiv [\omega_{129}, \Delta\omega_{129}, \omega_{131}]/(2\pi)$. These frequencies are shifted by 257.16, 1.17, and 76.24 Hz respectively for reasons of clarity. The B_z shift is relative to 21.92 μT. The fitted slopes of (a)–(c) are (11.74 ± 0.64), (0.000 ± 0.011), and (3.49 ± 0.19) mHz/nT. (d)–(f) Pump power dependence of the three measured frequencies with the fitted slopes (-1.57 ± 0.19), (0.075 ± 0.021), and (-0.452 ± 0.055) mHz/mW respectively. (g) Traces of 1000 successive FID measurements at zero gradient (PT-symmetric phase). The pump power changes among [40, 45, 50, 55, 60] mW periodically, and the color of points represents the value of pump power. The histogram on the right shows the distribution and average value of $\Omega_{\rm rot}^{(2\omega)}$ at 40, 50, and 60 mW. (h) The same as (g), but for 2000 successive FID measurements at $|G| = 250$ nT/cm (PT-broken phase). (i) The average values in (g) and (h). Solid and dashed lines are linear fitting of the data points. The slope of the blue solid line is (16.7 ± 2.0) μHz/mW, while that of the red dashed line is (0.0 ± 2.2) μHz/mW. Data points in (a)–(f) are the mean values of 400 repeated measurements.

precession frequencies $\boldsymbol{\omega} = [\omega_{129}, \omega_{131}]^{\rm T}$ of ^{129}Xe and ^{131}Xe nuclear spin to determine the rotation rate $\Omega_{\rm rot}$ of the system. The precession frequencies $\boldsymbol{\omega}$ depend on $\mathbf{x} = [B, \Omega_{\rm rot}]^{\rm T}$ through the relation $\omega_\alpha = \gamma_\alpha B + \Omega_{\rm rot}$, where γ_α is the gyromagnetic ratio of ^{129}Xe or ^{131}Xe nuclear spin and B is the magnetic field along the z direction. The rotation rate is estimated by (assume $B > 0$)

$$\Omega_{\rm rot}^{(2\omega)} \equiv \frac{|R\omega_{131}| - |\omega_{129}|}{1 + |R|}, \tag{5}$$

with $R \equiv \gamma_{129}/\gamma_{131} \approx -3.373417$ the ratio of gyromagnetic ratios [51].

The above relation $\omega_\alpha = \gamma_\alpha B + \Omega_{\rm rot}$ is only valid when the magnetic field B is spatially uniform. Because of the difference of boundary conditions and gyromagnetic ratios, the diffusive ^{129}Xe and ^{131}Xe spins can have different responses to a nonuniform magnetic field. The spin precession frequencies are actually $\omega_\alpha = \gamma_\alpha B_0 + \Omega_{\rm rot} + \gamma_\alpha \bar{B}_{{\rm A},\alpha}$, where $\bar{B}_{{\rm A},\alpha}$ is an isotope-dependent effective magnetic field originated from the inhomogeneity of $B(\mathbf{r})$ [52] and B_0 is the mean value of $B(\mathbf{r})$. The differential part $b_{\rm A} \equiv \bar{B}_{{\rm A},129} - \bar{B}_{{\rm A},131}$ of the isotope-dependent effective field produces a systematic error on the estimator Eq. (5) as

$$\Omega_{\rm rot}^{(2\omega)} - \Omega_{\rm rot} = -\frac{|\gamma_{129}\gamma_{131}|}{|\gamma_{129}| + |\gamma_{131}|} b_{\rm A}. \tag{6}$$

One origin of the inhomogeneity of $B(\mathbf{r})$ is the polarization field generated by the spin-exchange collisions between Xe and Rb atoms. In our experiment, the $\bar{B}_{{\rm A},\alpha}$ from the polarization field is in the order of $\sim 10^1$ nT, and the observed value of $b_{\rm A}$ can be as large as $\sim 10^0$ nT. More importantly, $b_{\rm A} = b_{\rm A}(P_{\rm pump}, f_{\rm pump}, T, \ldots)$ depends on several control parameters such as the laser power $P_{\rm pump}$, laser frequency $f_{\rm pump}$, and cell temperature T, etc. The drift of these control parameters will eventually limit the long-term stability of $\Omega_{\rm rot}$ measurement. Great efforts based on pulse control of the alkali-metal atoms have been made to eliminate the influence of the polarization field [53–55]. Here we demonstrate a new method utilizing the PT transition.

The PT transition extends the dual-species NMRG to a three-component comagnetometer. Particularly, we measure three frequencies $\boldsymbol{\omega} = [\omega_{129}, \Delta\omega_{129}, \omega_{131}]^{\rm T}$ as functions of three input variables $\mathbf{x} = [B_0, \Omega_{\rm rot}, P_{\rm pump}]^{\rm T}$, where $\omega_{129} \equiv (\omega_+ + \omega_-)/2$ and $\Delta\omega_{129} \equiv |\omega_+| - |\omega_-|$ are the mean frequency and the PT splitting of ^{129}Xe. As a proof-of-principle experiment, we assumed the pump power $P_{\rm pump}$ to be the dominating parameter which affects the nonuniform magnetic field, i.e., $b_{\rm A} = b_{\rm A}(P_{\rm pump})$. The Jacobian matrix is experimentally determined, and the gyroscope signal $\Omega_{\rm rot}^{(3\omega)}$ of the three-component comagnetometer is calculated by solving the following linear equation

$$\delta\begin{pmatrix}|\omega_{129}|\\ \Delta\omega_{129}\\ |\omega_{131}|\end{pmatrix}=\begin{pmatrix}|\gamma_{129}| & \chi_1 & -1\\ 0 & \chi_2 & 0\\ |\gamma_{131}| & \chi_3 & +1\end{pmatrix}\cdot\delta\begin{pmatrix}B_0\\ P_{\mathrm{pump}}\\ \Omega_{\mathrm{rot}}^{(3\omega)}\end{pmatrix},\quad(7)$$

where χ_1, χ_2, and χ_3 are the fitted slopes in Figs. 4(d)–4(f), respectively. The PT splitting $\Delta\omega_{129}$ is insensitive to B_0 but proportional to the change of P_{pump}. This can be understood by noticing that the spatial distribution of the polarization field relies on P_{pump}. The ^{129}Xe spins sense the change of the inhomogeneous polarization field and manifest it as the splitting $\Delta\omega_{129}$ between the two localized modes in the PT-broken phase.

Figures 4(g)–4(i) compare the measurement stability of Ω_{rot} against the change of P_{pump}. During the whole measurement, the actual rotation rate Ω_{rot} is unchanged. The traditional dual-species NMRG estimator $\Omega_{\mathrm{rot}}^{(2\omega)}$ shows a 17 μHz/mW dependence on P_{pump}, while the slope almost vanishes for our three-component comagnetometer estimator $\Omega_{\mathrm{rot}}^{(3\omega)}$. This result demonstrates the great potential for improving comagnetometer stability.

We have demonstrated the stability of a three-component comagnetometer against the fluctuation of pumping power, but the key idea is that we can choose two arbitrary parameters x_1 and x_2, and then configure the three-component comagnetometer to be stable against the fluctuation of both x_1 and x_2. x_1, x_2 can be any continuous scalar parameter of the experimental system such as laser power, laser wavelength, cell temperature, coil current, or even a linear combination of them. Because of the mode localization nature in the PT-broken phase, $\Delta\omega_{129}$ is directly sensitive to the nonuniform distribution of the magnetic field. Conversely, ω_{129} and ω_{131} are mainly determined by the average magnetic field; nonuniformity only contributes perturbative corrections. These make the $\Delta\omega_{129}$ a good indicator for monitoring the change of parameters that can induce nonuniform magnetic field, and then to suppress their influence on ω_{129} and ω_{131}.

Discussion and outlook.—In this Letter, we report the observation of the PT transition of diffusive nuclear spins. Particularly, the spin precession frequency splitting and the mode localization are measured in the PT-broken phase. In this phase, the boundary between coherent and incoherent spin motion is blurred. The random spin diffusion in a gradient field behaves like a coherent coupling (e.g., spin-orbit coupling) in a Hermitian system, rather than a pure dissipation as in the PT-symmetric phase. The diffusive nuclear spin system provides an excellent testbed for further exploring the non-Hermitian physics.

We also demonstrate the application of PT transition in the sensing of weak signals. The comagnetometer in the PT-broken phase is sensitive to the magnetic field gradient, which enables the design of the gradiometer [56,57] measuring the magnitude and gradient of the magnetic field in a single atomic cell. Furthermore, the PT transition was shown to be useful in improving the sensitivity of parameter estimation near the EPs previously [30–36], although the signal-to-noise ratio and the fundamental precession limit are still under debate [58–61]. Our Letter shows that, assisted by the PT transition, the spatial motion is engaged in the sensing process, and the sensor stability, another important aspect of high-precession measurement, is significantly enhanced. This paves the way to develop stable comagnetometers for the detection of extremely weak signals.

We thank Yanhua Wang for the assistance in establishing the experiment setup and Dawu Xiao for the preliminary theoretical calculations. We thank Kang Dai for providing the vapor cell. This work is supported by NSFC (Grants No. U2030209, No. 12088101, and No. U1930402). X. Z. and N. Z. designed the experiment. X. Z. performed the measurements and analyzed the data. J. H., N. Z., and X. Z. carried out the theoretical analysis and numerical simulation. N. Z. and X. Z. wrote the manuscript. N. Z. supervised the project.

nzhao@csrc.ac.cn

[1] D. Budker and M. Romalis, Optical magnetometry, Nat. Phys. **3**, 227 (2007).
[2] T. G. Walker and M. S. Larsen, Chapter Eight - Spin-Exchange-Pumped NMR Gyros, Adv. At., Mol., Opt. Phys. **65**, 373 (2016).
[3] M. Jiang, H. Su, A. Garcon, X. Peng, and D. Budker, Search for axion-like dark matter with spin-based amplifiers, Nat. Phys. **17**, 1402 (2021).
[4] H. Su, Y. Wang, M. Jiang, W. Ji, P. Fadeev, D. Hu, X. Peng, and D. Budker, Search for exotic spin-dependent interactions with a spin-based amplifier, Sci. Adv. **7**, eabi9535 (2021).
[5] H. Yan, G. A. Sun, S. M. Peng, Y. Zhang, C. Fu, H. Guo, and B. Q. Liu, Searching for New Spin- and Velocity-Dependent Interactions by Spin Relaxation of Polarized ^{3}He Gas, Phys. Rev. Lett. **115**, 182001 (2015).
[6] M. Bulatowicz, R. Griffith, M. Larsen, J. Mirijanian, C. B. Fu, E. Smith, W. M. Snow, H. Yan, and T. G. Walker, Laboratory Search for a Long-Range T-Odd, P-Odd Interaction from Axionlike Particles Using Dual-Species Nuclear Magnetic Resonance with Polarized ^{129}Xe and ^{131}Xe Gas, Phys. Rev. Lett. **111**, 102001 (2013).
[7] W. A. Terrano and M. V. Romalis, Comagnetometer probes of dark matter and new physic, Quantum Sci. Technol. **7**, 014001 (2022).
[8] E. L. Hahn, Spin echoes, Phys. Rev. **80**, 580 (1950).
[9] H. Y. Carr and E. M. Purcell, Effects of diffusion on free precession in nuclear magnetic resonance experiments, Phys. Rev. **94**, 630 (1954).
[10] H. C. Torrey, Bloch equations with diffusion terms, Phys. Rev. **104**, 563 (1956).
[11] S. D. Stoller, W. Happer, and F. J. Dyson, Transverse spin relaxation in inhomogeneous magnetic fields, Phys. Rev. A **44**, 7459 (1991).

[12] C. M. Bender and S. Boettcher, Real Spectra in Non-Hermitian Hamiltonians Having PT Symmetry, Phys. Rev. Lett. **80**, 5243 (1998).
[13] C. M. Bender, Making sense of non-Hermitian Hamiltonians, Rep. Prog. Phys. **70**, 947 (2007).
[14] K. G. Makris, R. El-Ganainy, D. N. Christodoulides, and Z. H. Musslimani, Beam Dynamics in PT Symmetric Optical Lattices, Phys. Rev. Lett. **100**, 103904 (2008).
[15] C. E. Rüter, K. G. Makris, R. El-Ganainy, D. N. Christodoulides, M. Segev, and D. Kip, Observation of parity–time symmetry in optics, Nat. Phys. **6**, 192 (2010).
[16] L. Chang, X. Jiang, S. Hua, C. Yang, J. Wen, L. Jiang, G. Li, G. Wang, and M. Xiao, Parity–time symmetry and variable optical isolation in active–passive-coupled microresonators, Nat. Photonics **8**, 524 (2014).
[17] B. Peng, S. K. Özdemir, F. Lei, F. Monifi, M. Gianfreda, G. L. Long, S. Fan, F. Nori, C. M. Bender, and L. Yang, Parity–time-symmetric whispering-gallery microcavities, Nat. Phys. **10**, 394 (2014).
[18] L. Feng, Z. J. Wong, R.-M. Ma, Y. Wang, and X. Zhang, Single-mode laser by parity-time symmetry breaking, Science **346**, 972 (2014).
[19] B. Zhen, C. W. Hsu, Y. Igarashi, L. Lu, I. Kaminer, A. Pick, S. L. Chua, J. D. Joannopoulos, and M. Soljačić, Spawning rings of exceptional points out of Dirac cones, Nature (London) **525**, 354 (2015).
[20] J. Doppler, A. A. Mailybaev, J. Böhm, U. Kuhl, A. Girschik, F. Libisch, T. J. Milburn, P. Rabl, N. Moiseyev, and S. Rotter, Dynamically encircling an exceptional point for asymmetric mode switching, Nature (London) **537**, 76 (2016).
[21] H. Xu, D. Mason, L. Jiang, and J. G. Harris, Topological energy transfer in an optomechanical system with exceptional points, Nature (London) **537**, 80 (2016).
[22] Z. Zhang, Y. Zhang, J. Sheng, L. Yang, M. A. Miri, D. N. Christodoulides, B. He, Y. Zhang, and M. Xiao, Observation of Parity-Time Symmetry in Optically Induced Atomic Lattices, Phys. Rev. Lett. **117**, 123601 (2016).
[23] Y. Li, Y. G. Peng, L. Han, M. A. Miri, W. Li, M. Xiao, X. F. Zhu, J. Zhao, A. Alù, S. Fan, and C. W. Qiu, Anti–parity-time symmetry in diffusive systems, Science **364**, 170 (2019).
[24] M. Schaden, K. F. Zhao, and Z. Wu, Effects of diffusion and surface interactions on the line shape of electron paramagnetic resonances in the presence of a magnetic field gradient, Phys. Rev. A **76**, 062502 (2007).
[25] K. F. Zhao, M. Schaden, and Z. Wu, Nonperturbative broadening of paramagnetic resonance lines by transverse magnetic field gradients, Phys. Rev. A **78**, 013418 (2008).
[26] K. F. Zhao, M. Schaden, and Z. Wu, Method for measuring surface-interaction parameters of spin-polarized Rb atoms on coated Pyrex glass surfaces using edge enhancement, Phys. Rev. A **78**, 034901 (2008).
[27] K. F. Zhao, M. Schaden, and Z. Wu, Enhanced magnetic resonance signal of spin-polarized Rb atoms near surfaces of coated cells, Phys. Rev. A **81**, 042903 (2010).
[28] Z. Wu, Wall interactions of spin-polarized atoms, Rev. Mod. Phys. **93**, 035006 (2021).
[29] B. Saam, N. Drukker, and W. Happer, Edge enhancement observed with hyperpolarized ^{3}He, Chem. Phys. Lett. **263**, 481 (1996).
[30] J. Wiersig, Enhancing the Sensitivity of Frequency and Energy Splitting Detection by Using Exceptional Points: Application to Microcavity Sensors for Single-Particle Detection, Phys. Rev. Lett. **112**, 203901 (2014).
[31] J. Wiersig, Sensors operating at exceptional points: General theory, Phys. Rev. A **93**, 033809 (2016).
[32] Z. P. Liu, J. Zhang, Ş. K. Özdemir, B. Peng, H. Jing, X. Y. Lü, C. W. Li, L. Yang, F. Nori, and Y. X. Liu, Metrology with PT-Symmetric Cavities: Enhanced Sensitivity near the PT-Phase Transition, Phys. Rev. Lett. **117**, 110802 (2016).
[33] W. Chen, Ş. Kaya Özdemir, G. Zhao, J. Wiersig, and L. Yang, Exceptional points enhance sensing in an optical microcavity, Nature (London) **548**, 192 (2017).
[34] H. Hodaei, A. U. Hassan, S. Wittek, H. Garcia-Gracia, R. El-Ganainy, D. N. Christodoulides, and M. Khajavikhan, Enhanced sensitivity at higher-order exceptional points, Nature (London) **548**, 187 (2017).
[35] Y. H. Lai, Y. K. Lu, M. G. Suh, Z. Yuan, and K. Vahala, Observation of the exceptional-point-enhanced Sagnac effect, Nature (London) **576**, 65 (2019).
[36] M. P. Hokmabadi, A. Schumer, D. N. Christodoulides, and M. Khajavikhan, Non-Hermitian ring laser gyroscopes with enhanced Sagnac sensitivity, Nature (London) **576**, 70 (2019).
[37] C. Cohen-Tannoudji, J. Dupont-Roc, S. Haroche, and F. Laloë, Various level crossing resonances on optically pumped atoms in zero field, Rev. Phys. Appl. (Paris) **5**, 95 (1970).
[38] E. J. Eklund, Microgyroscope based on spin-polarized nuclei, Ph.D. thesis, University of California, Irvine, 2008, Sec. III.1.
[39] F. Tang, A.-x. Li, K. Zhang, Y. Wang, and N. Zhao, Optimizations of a parametric-modulation atomic magnetometer in a nuclear magnetic resonance gyroscope, J. Phys. B **52**, 205001 (2019).
[40] K. Zhang, Z. Luo, F. Tang, N. Zhao, and Y. Wang, Experimental optimization of atomic magnetometer in nuclear magnetic resonance gyroscope, Jpn. J. Appl. Phys. **59**, 030907 (2020).
[41] B. Song, Y. Wang, and N. Zhao, Spin-polarization dependence of the Rb-Xe spin-exchange optical pumping process, Phys. Rev. A **104**, 023105 (2021).
[42] See Supplemental Material at http://link.aps.org/supplemental/10.1103/PhysRevLett.130.023201 for detailed theoretical explanation, which includes Refs. [43–49].
[43] W. Happer, Optical pumping, Rev. Mod. Phys. **44**, 169 (1972).
[44] T. G. Walker and W. Happer, Spin-exchange optical pumping of noble-gas nuclei, Rev. Mod. Phys. **69**, 629 (1997).
[45] S. J. Seltzer, Developments in Alkali-Metal atomic magnetometry, Ph.D. thesis, Princeton University, 2008.
[46] B. C. Grover, Noble-Gas NMR Detection through Noble-Gas-Rubidium Hyperfine Contact Interaction, Phys. Rev. Lett. **40**, 391 (1978).
[47] W. Zheng, H. Gao, J. G. Liu, Y. Zhang, Q. Ye, and C. Swank, General solution to gradient-induced transverse and longitudinal relaxation of spins undergoing restricted diffusion, Phys. Rev. A **84**, 053411 (2011).

[48] B. E. Poling, J. M. Prausnitz, and J. P. O'Connell, , *The Properties of Gases and Liquids*, 5th ed. (McGraw-Hill Education, New York, 2001).

[49] Y. K. Feng, S. B. Zhang, Z. T. Lu, and D. Sheng, Electric quadrupole shifts of the precession frequencies of ^{131}Xe atoms in rectangular cells, Phys. Rev. A **102**, 043109 (2020).

[50] The error bars in all figures of this Letter represent the 95% confident intervals of experiment data.

[51] W. Makulski, ^{129}Xe and ^{131}Xe nuclear magnetic dipole moments from gas phase NMR spectra, Magn. Reson. Chem. **53**, 273 (2015).

[52] D. Sheng, A. Kabcenell, and M. V. Romalis, New Classes of Systematic Effects in Gas Spin Comagnetometers, Phys. Rev. Lett. **113**, 163002 (2014).

[53] M. E. Limes, D. Sheng, and M. V. Romalis, ^{3}He – ^{129}Xe Comagnetometery using ^{87}Rb Detection and Decoupling, Phys. Rev. Lett. **120**, 033401 (2018).

[54] A. Korver, D. Thrasher, M. Bulatowicz, and T. G. Walker, Synchronous Spin-Exchange Optical Pumping, Phys. Rev. Lett. **115**, 253001 (2015).

[55] D. A. Thrasher, S. S. Sorensen, J. Weber, M. Bulatowicz, A. Korver, M. Larsen, and T. G. Walker, Continuous comagnetometry using transversely polarized Xe isotopes, Phys. Rev. A **100**, 061403(R) (2019).

[56] D. Sheng, A. R. Perry, S. P. Krzyzewski, S. Geller, J. Kitching, and S. Knappe, A microfabricated optically-pumped magnetic gradiometer, Appl. Phys. Lett. **110**, 031106 (2017).

[57] R. Zhang, W. Xiao, Y. Ding, Y. Feng, X. Peng, L. Shen, C. Sun, T. Wu, Y. Wu, Y. Yang, Z. Zheng, X. Zhang, J. Chen, and H. Guo, Recording brain activities in unshielded Earth's field with optically pumped atomic magnetometers, Sci. Adv. **6**, eaba8792 (2020).

[58] W. Langbein, No exceptional precision of exceptional-point sensors, Phys. Rev. A **98**, 023805 (2018).

[59] M. Zhang, W. Sweeney, C. W. Hsu, L. Yang, A. D. Stone, and L. Jiang, Quantum Noise Theory of Exceptional Point Amplifying Sensors, Phys. Rev. Lett. **123**, 180501 (2019).

[60] H. K. Lau and A. A. Clerk, Fundamental limits and non-reciprocal approaches in non-Hermitian quantum sensing, Nat. Commun. **9**, 4320 (2018).

[61] C. Chen, L. Jin, and R. B. Liu, Sensitivity of parameter estimation near the exceptional point of a non-Hermitian system, New J. Phys. **21**, 083002 (2019).